

The Geometry and Motion of Nematode Sperm Cells

Evgeny Demekhin

Moscow State University

Nicole Haugen

Bemidji State University

Brian Ibanez

Andrews University

Jerome Lederman

Preuss School, University of California, San Diego

Kaitlyn Murphy

Montclair State University

***Diana Verzi**

San Diego State University

Debra Witczak

Illinois State University

January 14, 2009

Corresponding author: Dr. Diana W. Verzi, San Diego State University
720 Heber Avenue Callexico CA 92231
verzi@math.sdsu.edu 760-768-5531

Abstract

The nematode sperm cell crawls by recycling major sperm protein (MSP) from dimers into subfilaments, filaments, and filament complexes, as a result of thermal writhing in the presence of hydrophobic patches. Polymerization near leading edges of the cell intercolates MSP dimers onto the tips of growing filament complexes, forcing them against the cell boundary, and extending the cytoskeleton in the direction of motion. Strong adhesive forces attach the cell to the substrate in the forward part of the lamellipod, while depolymerization in the rearward part of the cell breaks down the cytoskeleton, contracting the lamellipod and pulling the cell body forward.

The movement of these cells, then, is caused by coordinated protrusive, adhesive and contractile forces, spatially separated across the lamellipod. This paper considers a phenomenological model that tracks discrete elements of the cytoskeleton in curvilinear coordinates. The pseudo-two dimensional model primarily considers protrusion and rotation of the cell, along with the evolution of the cell boundary. General assumptions are that pH levels within the lamellipod regulate protrusion, contraction and adhesion, and that growth of the cytoskeleton, over time, is perpendicular to the evolving cell boundary. The model follows the growth and contraction of a discrete number of MSP fiber complexes, since they appear to be the principle contributors for force generation in cell boundary protrusion and contraction, and the backbone for the dynamic geometry and motion.

Key words: cell shape, cytoskeleton, cell motility, major sperm protein, MSP

1 Introduction

The motility of specific animal cells plays an integral role in many biological processes. For example, whenever an animal tissue is damaged, fibroblasts crawl to the site to repair the

wound. Tracking down foreign pathogens and eliminating them, along with the threat they present to the body, is the work of motile neutrophils. However, not all motile cells are beneficial. Metastatic cancer cells crawl to invade distant areas of the body, enabling the disease to spread. A thorough understanding of how animal cells accomplish movement is, therefore, highly desirable in the field of medicine, and there is considerable interest in modeling cell motility.

All crawling cells move by the same basic processes: Protruding near the leading edge, adhering to the surface, and contracting at the rear to pull the cell body forward. However, complications quickly arise when examining these processes more closely. In most eukaryotic cells, the main players in cellular movement are actin and myosin [Borisy and Svitkina, 2000]. In addition to providing the basis of cell motility, these structures also function in the processes of phagocytosis, movement of vesicles and organelles, surface rearrangement, and cytokinesis. Actin and myosin require accessory proteins for each specific activity, creating highly interconnected and complex systems [Mogilner and Oster, 1996]. It becomes difficult to untangle this complexity to determine what contributes to cell motility in these multi-functional protein complexes.

Motile spermatozoa of the nematode *Ascaris suum* (*A. suum*) crawl like amoebae with the aid of a motile appendage called a lamellipod [Roberts and Stewart, 1995]. The cytoskeleton consists primarily of a Major Sperm Protein (MSP) gel network, so that studying *A. suum* may avoid many of the complications associated with actin-based motility [Mogilner and Verzi, 2003]. In *A. suum*, many cellular components such as the endoplasmic reticulum, the Golgi apparatus, and the usual actin cytoskeleton are left behind in the residual body after meiosis [Italiano et al., 1996]. The result of this process is a cell that is dedicated almost entirely to locomotion, providing us with a relatively straightforward system for studying cell motility. While simplified, the cytoskeletal dynamics of *A. suum* employ similar physical principles to generate motility as the more complex actin-based systems [Mogilner, 2008].

In the cell's lamellipod, MSP is organized into 15 – 20 branched fiber complexes that extend backward from the leading edge to the rear of the cell. This network of crosslinked bundles forms the cytoskeleton and shapes the lamellipod [Sepsewol and Taft, 1990]. Protrusion is accomplished at the leading edge of the cell by polymerization reactions in the cytoskeleton that exert sufficient force to push the gel forward [Wolgemuth et al., 2004]. Polymerization

refers to the process of adding MSP units to filament tips through a nucleation-elongation reaction [Italiano et al., 2001]. At various locations along the leading edge of the lamellipod two proteins, a membrane protein (MSP Polymerization Organizing Protein or MPOP) and a cytosolic protein (MFP2), come together to create a nucleation complex that catalyzes the polymerization reaction [LeClaire et al., 2003; Yi et al., 2007]. Studies have shown that the rates of elongation of MSP filaments fall sharply at a distance of about $0.5\mu\text{m}$ from the nucleation complex, indicating that polymerization only occurs in close proximity [LeClaire et al., 2003; Miao et al., 2003]. As newly polymerized filaments flow backward from the edge of the lamellipod and out of this elongation region, they self assemble into a crosslinking fiber complex [LeClaire et al., 2003]. It is interesting to note that the concentration of the cytosolic protein, rather than the amount of MSP, limits the rate of fiber growth [Yi et al., 2007]. In vitro experiments have shown that MSP polymerization will keep pace with the translocation of the nucleation complex [Italiano et al., 1996], corresponding to the rate of protrusion of the leading edge. Fig. 1 identifies key structures of the crawling cell from top and side views.

While protrusion is accomplished by MSP polymerization at the front of the cell, contraction is thought to be driven by depolymerization of the assembled cytoskeletal network at the rear. In vitro experiments involving the addition of *Yersinia Enterocolytica* Tyrosine Phosphatase (YOP) showed a marked decrease in the length and optical density of MSP filaments from *A. suum*. YOP appears to cause fibers to switch from growth to retraction mode by altering tyrosine phosphorylation of key components in the cytoskeletal system. In vivo experiments with the sperm of *A. suum* display similar bundle retraction and loss of optical density when treated with a sodium acetate-HKB buffer to lower cytoplasmic pH [Miao et al., 2003]. These and other in vitro experiments have led to the proposal that forward movement of the cell body in *A. suum* is accomplished by cytoskeletal retraction, without the assistance of motor proteins [Zajac et al., 2008; Miao et al., 2003].

Adhesion, or the attachment of the lamellipod to the substrate, is believed to play an integral role in generating forward motion. It is strong at the leading edge and diminishes toward the rear of the cell, with almost no measurable adhesive contact beneath the cell body. This is a critical property for cell motility, since without it the processes of extension and contraction would merely recycle the MSP cytoskeleton and accomplish no forward motion

[Mogilner, 2008]. With graded adhesion, contractile forces pull up the adhesive sites at the rear of the cell while protrusion lays down new sites at the front, resulting in a continuous cycle of attachment-detachment between the lamellipod membrane and the substrate to generate forward motion [Roberts and King, 1991].

The interior pH appears to regulate almost every facet of motility in nematode sperm crawling. A gradient that decreases from the front to the rear is maintained, with the leading edge approximately 0.2 units higher [Mogilner and Oster, 2008]. The origin of this gradient is unknown, but it is conjectured that protons from mitochondria diffuse across the lamellipod [Mogilner and Verzi 2003]. While the molecular mechanisms for adhesion have not yet been identified [Zajac et al., 2008], attachment to the substrate appears to be regulated in part by pH: Adhesion is stronger at a higher pH away from the cell body and weaker in the more acidic environment near the lamellipod-cell body interface. Graded pH may also play a role in spatially separating protrusion and contraction, by acting as an on/off switch for critical proteins involved in these processes. LeClaire et al. [2003] identified a major sperm protein polymerization organizing protein (MPOP) as the only membrane component required to nucleate MSP polymerization under physiological conditions. While present throughout the lamellipod, MPOP is activated to nucleate MSP polymerization only in areas where it undergoes a pH-sensitive tyrosine phosphorylation. Antiphosphotyrosine labeling and confocal fluorescent microscopy have identified activated MPOP primarily at the tips of filament bundles, along the edge of the lamellipod [LeClaire et al., 2003]. Similarly, the pH gradient may play an indirect role in cytoskeletal disassembly and retraction by activating a phosphatase that would in turn activate a yet-to-be determined protein to trigger fiber bundle depolymerization [Miao et al., 2003]. The sideview of the crawling cell in Fig. 1 suggests a spatial separation between these processes, regulated by a graded pH-field.

Bottino et al. [2002] developed a quantitative two dimensional (2D) model of the crawling cell which considered the lamellipod as an isotropic, dynamic domain. Simulations using finite elements produced stable moving shapes resembling those of the motile cells. However, computer simulations of full 2D models are time consuming, and finite-element methods preclude the important localized view of MSP dynamics. Conversely, Mogilner and Verzi [2003] developed a more complex continuum model in one dimension (1D) for motility in *A. suum* that considered motion as a result of friction and physical stress as MSP cycled

between the states of free-floating dimers and fiber bundles. Their work considered a single MSP bundle in the anterior-posterior direction across the motile cell. Simulations using finite differencing captured local dynamics and recovered the stable forward motion and speed of in vitro observations. However, the 1D model could not consider important processes at the lateral sides of the cell involved in cell-shape maintenance and turning.

For a geometric perspective, Lee et al. [1993] proposed that fish epidermal keratocytes accomplished a smooth, gliding motion while maintaining cell shape through GRE, or localized growth of the lamellipod perpendicular to the evolving edge of the cell. In observing videos for crawling nematode sperm cells [Roberts and Stewart, 2000; Zajac et al, 2008], we note that MSP bundles likewise intersect the edge of the cell at right angles, whether at the front or lateral sides of the lamellipod. In this paper, we develop a pseudo-2D model for the nematode sperm cell, to consider the role of bundle protrusion in motion and cell geometry for extension, steady-state crawling and turning. We assume that bundle protrusions occur orthogonal to the cell’s edge over time, and that the rate of protrusion, or polymerization and bundling, is regulated by a linear pH gradient. The model simulates the graded radial extension (GRE) hypothesis [Lee et al., 1993] and introduces a protrusion function that acts in concert with a contraction-polymer recycling algorithm to recover the geometry and motion of crawling cells observed in recent experiments [Miao et al., 2003; Roberts and Stewart, 1995; Zajac et al., 2008]. Since there are only 15-20 bundles observed in the lamellipod of *A. suum*, a continuum model in the curvilinear coordinate system for each bundle eliminates excessive computation time over a full 2D model while examining the local effects each bundle has upon the evolving contour of the motile cell. The model is developed in Methods, with simulations for steady-state crawling, turning and cell shape maintenance in Results. The implications of the model and simulations are drawn in Conclusions, and suggestions for continued work may be found in Discussion.

2 Methods

We assume the nematode sperm cell’s motion and the evolving shape of its contour are driven, primarily, by the growth of its cytoskeletal elements, orthogonal to the cell’s edge, and that growth and motion are regulated by a spatial pH distribution, and restricted by

the availability of membrane proteins. We consider the cell as an elliptically shaped cell body, riding atop its lamellipod, and model the forward half of this ellipse from the center line of rotation for a turning cell. The lamellipod is composed of a series of rigid filaments, or cytoskeletal bundles, that are held together by a viscous gel. It is extended by graded cytoskeletal growth, in combination with adhesive interaction between hydrophobic nodal points along MSP structures and the surface over which the cell crawls. Protrusion and adhesion near the front of the cell occur at the same time that contraction from solution of cytoskeletal bundles occurs at the rear, where the leading edge of the cell body meets the trailing edge of the lamellipod. Cytoskeletal growth perpendicular to the cell's contour is described by a differential equation of the form

$$\frac{\partial \vec{r}_i}{\partial t} = v_i \vec{n}_i, \quad (1)$$

where r_i is the position vector for the cytoskeletal element i , v_i is the velocity of protrusion and \vec{n}_i is a vector normal to the cell's contour for each cytoskeletal element i . In this paper, we emphasize the magnitude and direction of protrusion and do not explicitly consider retrograde flow. Instead, we utilize a contraction-dimer recycling algorithm that assumes polymerization and depolymerization are balanced when the cell is crawling with steady-state speed and shape.

Suppose that protrusion is regulated by pH, and a more basic environment is necessary to activate a vesical protein lodged in the membrane of the lamellipod. Protons from mitochondria diffuse throughout the lamellipod, and concentrations relax to a steady-state rapidly relative to the time scale for cell crawling. An order one approximation predicts the proton concentration decreases exponentially with distance from the cell body. Since pH is a negative log function of this concentration, it may be approximated to increase linearly with distance from the cell body. (See Appendix B in [Mogilner and Verzi, 2003] for a more detailed derivation):

$$pH_{t_i}(x_{t_i}) = 6.2 + \frac{\alpha x_{t_i}}{l(t)}. \quad (2)$$

Here α is a scaling parameter, x_{t_i} is the distance from the cell body to the tip of cytoskeletal element i , and $l(t)$ is the length of the central bundle protruding in the direction of motion at time t . This function allows internal pH to vary from 6.2 at the rear of the cell to 6.4 near the leading edge. While the pH varies linearly over the length of the lamellipod, the rate of

change in protrusion over time is governed by a nonlinear chemical process that decreases slowly with distance from cell body and [respectively] higher pH values:

$$v_{t_i}(pH_{t_i}) = 5\gamma l(t)(pH_{t_i} - 6.2)e^{-25\lambda l(t)(pH_{t_i} - 6.2)^2}. \quad (3)$$

The parameter γ affects the optimal velocity and λ is the decay rate. As the tips of fiber bundles translocate in space, their protrusion rates vary over time, so that the spatial pH gradient ultimately regulates displacement in Eq. (1) and, ultimately, the shape of fiber bundles and the contour of the crawling cell.

We assume that cytoskeletal bundles dissolve in the more acidic conditions near and under the cell body and release their dimer composition back into the gel. Further, we suppose the direction of motion is governed by (user defined) symmetric or asymmetric contraction of the lamellipod at the cell body interface. When the lamellipod is extended enough to pull the cell body forward, we assume the cell body's motion, at each time step, is in the (preprogrammed) direction of motion at the average velocity of existing cytoskeletal bundles:

$$v_{cb}(t) = \frac{1}{n} \sum_{i=1}^n v_{t_i}(pH_{t_i}). \quad (4)$$

Rotation of the cell is assumed to occur in response to a change in the internal pH, probably from a change in the external environment [Miao et al., 2003]. As the cell body rotates, along with its contributing mitochondrial protons, so does the internal pH described in Eq. (2), altering the direction of motion for the velocity function in Eq. (3): Rotation of the axis for the cell body interface alters the calculation of x_{t_i} , which in turn alters v_{t_i} , and (over time) the shape of the lamellipod.

Suppose the cell body interface takes the initial shape of an ellipse, with its major axis parallel to the Cartesian y -axis. Then, the initial condition

$$\frac{x^2}{k^2} + y^2 = 1 \quad (5)$$

represents the elliptic edge of the cell body, where the parameter k affects its curvature. Initial points on the ellipse are determined by dividing the angle π (180 degrees) into equal sub-angles (θ_{0_i}), determined by the number of bundles to be simulated. Rays from the

Cartesian origin are connected to (x, y) coordinates on the ellipse where nucleation complexes initiate polymerization and bundle growth:

$$y_{0_i} = \tan(\theta_{0_i})x_{0_i} \quad (6)$$

$$x_{0_i} = \frac{k}{\sqrt{1 + k^2 \tan^2(\theta_{0_i})}}. \quad (7)$$

Dimers intercollate onto the growing tips of bundles at the edge of the cell, so that they appear to grow inward while pressure on the gel forces the membrane outward. To locate coordinates for intercollation normal to the local contour in the virtual cell, we approximate the slope of the tangent line at (x_{t_i}, y_{t_i}) as

$$m_{t_i} = \frac{x_{t_{i+1}} - x_{t_{i-1}}}{y_{t_{i-1}} - y_{t_{i+1}}}, \quad (8)$$

and calculate the cosine and sine of the angle this secant line makes with the x -axis

$$\cos(\theta_{t_i}) = \frac{1}{\sqrt{1 + m_{t_i}^2}} \quad (9)$$

$$\sin(\theta_{t_i}) = \frac{m_{t_i}}{\sqrt{1 + m_{t_i}^2}}. \quad (10)$$

We then use a discretized form of Eq. (1), expressed in terms of x and y , to locate the new tip of the protruding bundle for τ , the numerical timestep.

$$x_{(t+1)_i} = x_{t_i} + v_{t_i} \cos(\theta_{t_i}) \tau \quad (11)$$

$$y_{(t+1)_i} = y_{t_i} + v_{t_i} \sin(\theta_{t_i}) \tau. \quad (12)$$

Fig. 2 demonstrates why bundles appear to bend over time as the cell treadmills forward and elements within the the cytoskeleton move rearward with respect to the cell body. If the three curves shown in Fig. 2 represent the evolving cell edge, consider a membrane protein intercollating a dimer onto the tip of a bundle perpendicular to the inner curve at time $t = j$. Over time, the tip of the bundle advances rearward as the membrane advances forward due to graded protrusion, and contraction pulls the rear of the cell forward. At time $t = j + 1$, the bundle intersects the edge of the cell at the middle contour and the bundle tip appears to have glided along the side of the cell. The membrane protein again intercollates a

dimer onto its tip perpendicular to the evolving cell edge. By the time a dimer is intercollated perpendicular to the outer contour at time $t = j + 2$, the bending profile of the bundle is apparent. As the cell body glides forward, the distance from the tip of each bundle to the cell body interface decreases, and the change in pH slows the rate of protrusion, or dimer intercollation, for that bundle. Dimer intercollation is repeated at an ever decreasing rate over time for each bundle as it proceeds rearward, until it is assumed to be depolymerized in the more acidic environment near the cell body interface.

Biologists observe that the number of cytoskeletal elements appears relatively constant over time for an individual crawling cell [Sepenswol and Taft, 1990]. We, therefore, fix the number of bundles over time and utilize a contraction-polymer recycling algorithm to model the breakdown of bundles at the rear of the cell into dimers available for polymerization in the more basic environment away from the cell body. In Fig. 2, the membrane protein at point d initiates growth of a new bundle when the bundle at point b is depolymerized near the cell body. We assume membrane proteins are uniformly distributed across the lamellipod and available to initiate bundle growth at that point along the edge of the cell where distance between adjacent bundles is at a maximum, locating the membrane protein for this new point using parabolic interpolation.

3 Results

In this section, we simulate the evolving geometry of a crawling nematode sperm cell, utilizing the assumptions and model described above. We consider extension of the lamellipod, cell motion to steady-state crawling, cell shape maintenance, and turning to a pre-determined angle of rotation. The algorithm to effect motion initially extends the lamellipod, until it is of sufficient length to pull the cell body forward, approximately the diameter of the cell body. Then the cell body moves in the direction of motion dictated by the pH gradient, so that the velocity of contraction is assumed equal to the average of bundle protrusion velocities. As in Wolgemuth et al. [2005], we do not represent the cell body explicitly, but consider it to be at the tail end of contracting and depolymerizing bundles in simulation. The front half of the cell body is drawn in the following figures to facilitate visualization.

In our first simulation, we model extension of the lamellipod and approach to steady-

state shape and speed for the crawling cell. We normalize the cell to one dimensionless unit equals $10\mu\text{m}$, or the length of the minor axis for an elliptic cell body with a midrange of curvature (k in Eq. (5)). To increase computation time, we set one dimensionless video time frame equal to 8 seconds. Fig. 3 displays the results for nonlinear protrusion normal to the edge of the cell at $t = 4, 14, 24$ and 30 . In Fig. 3A, the lamellipod has extended, but the cell body has not moved from its initial position. In Figs. 3B and 3C, the lamellipod has reached steady-state shape and the cell body has moved 4 dimensionless units. At $t = 30$ in Fig. 3D, the cell has moved a little more than 5 spatial units, or 2.5 times its overall length. Converting to physical units, the cell body moved approximately $52\mu\text{m}$ in 208 seconds (after extension), for an average crawling speed of $15\mu\text{m}$ per minute.

In our next simulation, we consider the effect of different cell body shapes and sizes for the steady-state lamellipodial shape and speed for the crawling cell, as in Zajac et al. [2008]. The parameter k in Eq. (5) affects the initial shape of the assumed cell-body interface, and we wish to test the consistency of our equations for small perturbations in the initial conditions. Fig. 4 graphs three different simulations over 30 dimensionless time units for three different initial curvatures. Slides on the left side of Fig. 4 graph bundle extension without cell body translocation at $t = 4$, and slides on the right side graph translocation and steady-state shape after 30 time units. In Fig. 4A, bundles are clustered in the direction of motion at extension, and this phenomenon persists into steady state, in spite of the algorithm to recycle bundles at the point along the cell edge with maximum radial distance between existing bundles. The elliptic curvature of the cell body interface appears almost flat for this value of k , so that contour length is minimized and bundle density is maximized with this initial configuration. Fig. 4B graphs results for midrange curvature, which reduces bundle clustering in the direction of motion, and delivers the maximal crawling velocity. Fig. 4C graphs results for a cell body with a large amount of curvature, maximizing initial contour length, and the bundle density appears relatively uniform from extension to steady-state. However, this configuration reduces crawling velocity slightly when compared with minimal and midrange curvature results. While qualitatively similar, each initial condition produces a unique steady-state contour as a result of bundle recycling to maximize stiffness of the cytoskeleton over time.

Fig. 5 displays four still shots taken from a video of a turning cell in *A. suum*. The cell

in this video executes a spontaneous turn, since there is no obstruction to block its initial direction of motion. Fig. 5A displays the cell just before rotation, with a small protrusion on one lateral side of the lamellipod. In 5B, the cytoskeleton is breaking down on the right side of the cell and a contraction is initiated near the cell body (dark area). In Fig. 5C, the cell body begins to rotate toward its new direction of motion as protrusion continues across from it to establish a new leading edge. In Fig. 5D, the cell has almost completed its turn. Note the steady-state rectangular shape of the lamellipod, extending to the new direction of motion. The full video for this turning cell may be found at www.rohan.sdsu.edu/~dverzi (provided by T. M. Roberts of Florida State University). A link to a video on crawling in *Caenorhabditis elegans* (*C. elegans*) may also be found there (provided by C. Wolgemuth from University of Connecticut Health Center).

Observations of turning cells suggest that a small asymmetric contraction and protrusion at the rear of the lamellipod precedes a rotation of the cell body, followed by a rapid relocation of fiber bundles to re-establish the steady-state shape of the lamellipod in the new direction of motion. We next program a rotation of the cell body at $t = 12$, to simulate an asymmetric contraction, and observe our virtual cell's response in protrusion and direction of motion. Fig. 6 graphs the evolving contour of the turning cell after rotation of the cell body interface, and corresponding rotation of the pH gradient in Eq. (2). Figs. 6A and 6B indicate steady-state extension and crawling in the direction of the x-axis. However, in Fig. 6C, symmetry of the lamellipod has been broken, as bundles on the left side are longer. Since the rate of protrusion is a function of pH in Eq. (3), the rotation has affected the direction for graded radial extension. In Fig. 6D, bundles on the left half of the cell are noticeably longer, and two new bundles have formed there. Bundles on the right side have stopped growing, and cell body translocation has caused them to shorten. Bundles have begun to bend away from the newly established leading bundle that is extending in the new direction of motion. Video of simulations found in this section may be found at www.rohan.sdsu.edu/~dverzi. A flowchart explaining user interface, along with the *MATLAB* program, are also available there for download.

4 Conclusions

The phenomenological model for bundle growth and recycling supports in-vitro observations of bundle bending and retrograde flow, steady crawling and turning for spermatozoa in *A. suum*. It provides a geometric platform in curvilinear coordinates to test more complex models for discrete cytoskeletal elements in cell migration. The model does not consider physical stresses to induce contraction and adhesion, and how coordination of protrusion with these processes results in the steady gliding motion of nematode sperm cells. Retrograde flow of fiber bundles is accomplished through a contraction-polymer recycling algorithm, rather than computed with physical principles as in Mogilner and Verzi [2003]. Nevertheless, the model contributes to an evolving theory for cause and effect in 2D cell migration, with particular emphasis on filament bending along the lateral sides of the lamellipod and the contribution these components make to cell shape maintenance, a topic of study suggested in Mogilner’s review article [2008].

The function for rate of protrusion imposes graded intercollation of dimers on the growing ends of discrete bundles. The growth rate and direction for each bundle vary over time, and are dependent upon the distance from the tip of the bundle to the cell body and the evolving shape of the local contour, respectively. Simulations in this paper return cell observed geometries and bundle bending [Roberts and Stewart, 2000; Zajac et al., 2008], and support the GRE hypothesis [Lee et al., 1993], maximizing the tip of the bundle’s resistance to osmotic pressure [Mogilner and Oster, 2003; Wolgemuth et al., 2004]. While this was proposed for cell shape maintenance in crawling keratocytes, we believe this is the first time it has been tested in simulation to reproduce the overall rectangular shape of the lamellipod in crawling nematode sperm cells.

Roberts and King [1991] concluded that only the fiber complexes in a limited sector at the leading edge of the lamellipod undergo continuous elongation, while fibers outside that region become displaced toward the sides and eventually stop growing as the cell moves forward over them. In our simulations for cells moving parallel to the x-axis, growth persists for bundles that extend towards the center of the leading edge, and bundles along the lateral sides bend and reduce their rate of growth as treadmilling decreases their distance from the growing tip to the cell body. In Fig. 5, the turning cell establishes a new direction of motion, and a new region for continuous growth, along with new regions for bundle bending at the

lateral sides.

The assumption that the cell body moves at the average speed of bundle growth (Eq. (4)) assumes a continuous flow of available dimers, resulting from depolymerization and contraction at the rear, consistent with a continuum model based on conservation of momentum [Mogilner and Verzi, 2003]. Bundles along the lateral sides of the lamellipod grow slower than the advancing cell body so that they appear to move backward over time, until they are depolymerized. This retrograde flow, growth normal to the local contour, and the nonlinear growth rate in Eq. (3) are the components that give the virtual lamellipod its roughly rectangular shape and the fiber bundles their bending profile, similar to experimental observations.

Rather than assuming conservation of total MSP in various states from dimer to fiber complex, we assume conservation of bundles, initiating a new bundle when one is depolymerized. We assume MPOP proteins are distributed uniformly across the lamellipod, and available for activation by a cytoplasmic protein to initiate a new site for polymerization, bundling and protrusion whenever a bundle is absorbed under the advancing cell body. The new activation site is based on greatest distance between existing bundles, in response to comments in the literature that the cytoskeleton is dense across the lamellipod [Roberts and Stewart, 2000]. With the above assumptions, simulations in this paper demonstrate a steady-state motion of approximately $15\mu\text{m}/\text{minute}$, and cell geometries consistent with experimental observations for *A. suum* spermatozoa [Roberts and Stewart, 2000]. Variations in speed in Fig. 4, based on curvature of the cell body and the length of its interface with the lamellipod, suggest a relationship between contour shape/size and velocity, consistent with laboratory measurements and simulations for spermatozoa from the nematode *Caenorhabditis elegans* (*C. elegans*) [Zajac et al., 2008].

In vitro observations of turning in nematode sperm cells document a bulge that forms on a lateral side which shortly thereafter becomes the new leading edge, so that growth is more rapid on that side, and arrested on the opposing side. [Roberts and Stewart, 1995; Sepsenwol and Taft, 1990]. Our simulation for cell turning assumes an asymmetric contraction occurs from asymmetric depolymerization, and the cell body rotates behind the contraction, based on the notion of motion control from the rear in nematode sperm [Bottino et al., 2002; Mogilner and Verzi, 2003], mediated by rotation of a proton source in the mitochondria.

The simulated rotation of the cell body in Fig. 5 also rotates the pH function in Eq. (2) with respect to the crawling surface, causing a relocation of bundles that continue to grow, and bending bundles that treadmill rearward, decreasing their rate of growth with distance from the cell body. The evolving profile for the turning cell is consistent with in vitro videos for spermatozoa of *A. suum* [Roberts and Stewart, 2000; Italiano et al., 2001], and with comments in the literature that the formation of fiber complexes are integral in determining the location of new surface protrusions and thereby the direction of motion [Roberts and Stewart, 1995].

5 Discussion

To reproduce geometry and motion for cell migration in *A. suum*, we concentrated on contributions from the more rigid fiber complexes or bundles. With pH-regulated bundle growth perpendicular to the evolving membrane of the lamellipod, the treading cytoskeleton accomplishes forward translocation, filament bending and contour patterns observed in experimental laboratories. The phenomenological model does not directly consider diffusion of dimers, mechanics of contraction, and substrate adhesion, but rather builds their contribution implicitly into the algorithm or assumes their sufficient presence. Polymerization and depolymerization, and the associated forces of extension and contraction, are coupled [Italiano et al., 1999; Wolgemuth et al., 2005; Zajac et al., 2008], and in steady-state motion, the rate of dimer polymerization and bundling must equal the rate of depolymerization and unbundling. We reason that polymerization results in motion of the forward boundary and depolymerization in translocation of the rear boundary, so that equal rates of these processes should result in equal velocities of protrusion and contraction. This lead us to model cell body motion as the average of bundle protrusions once the lamellipod is of sufficient length to translocate the cell body.

In steady-state crawling, symmetric contractile forces seem to originate under the cell body and extend into the region just in front of the lamellipodial interface. Unfortunately, the opaque nature of the cell body inhibits observation of lamellipodial dynamics beneath it. However, when we observe videos for spontaneous turning in *A. suum* [Roberts and Stewart, 2000], assymmetric protrusion and contraction appear to occur simultaneously and

across from each other. The turn begins as a small bulge on a lateral side near the cell body, with a shadowed area of contraction of similar size near the cell body on the opposite side. On the other hand, Sepsenwol and Taft [1990] document a sperm from *A. suum* turning in response to contact with an obstacle in its path. Still shots from a video-DIC sequence display little contraction on the lateral side of a lamellipod when it contacts another sperm cell. Instead, the slides seem to indicate that the lamellipod contracts front-to-rear, as it simultaneously extends the side opposite the contact point to establish a new leading edge and a new direction of motion. Rotation of the cell body appears to be primarily in response to the forces of protrusion. Sepsenwol and Taft [1990] also comment on observations of sperm altering their direction when another sperm passes by, even without contact.

For a next step for the modeling process, we suggest a 2D mechanical model to extend the work of Mogilner-Verzi [2003] for conservation equations that track densities of cytoskeletal bundles, free MSP dimers and attachment nodes, or hydrophobic patches. A continuum model built on this platform in curvilinear coordinates that considers longitudinal distance from the cell body and angular distance from the direction of motion could provide new insights into the 2D nature of pH regulation and the coupling between extension and contraction. One might additionally test how changes in the external environment may cause the cell to change direction by varying boundary conditions. Many open questions remain in modeling cell migration. For example, what is the stimulus that initiates motion; how do elements in the external medium affect cell signalling, or what is the chemical/biological connection for pH regulation? It seems for every answer, one gets two new questions. Nevertheless, each answer helps us to better understand this complex phenomenon.

6 Acknowledgements

The authors thank Dr. T. M. Roberts from Florida State University for videos of cell turning for spermatozoa of *A. suum*, and Drs. Charles Wolgemuth and Mark Zajac from the University of Connecticut Health Center for migration videos for spermatozoa of *C. elegans*. This research was supported by the National Science Foundation REUT grant 0647384 at San Diego State University.

References

- [1] Borisy, GG, and Svitkina, TM. 2000. Actin machinery: Pushing the envelope. *Curr. Opin. Cell Biol.* 12:104-112.
- [2] Bottino D, Mogilner A, Roberts T, Stewart M, Oster G. 2002. How nematode sperm crawl. *J. Cell Science* 115-2:431-453.
- [3] Italiano J, Roberts T, Stewart M, Fontana C. 1996. Reconstitution in vitro of the motile apparatus from the amoeboid sperm of *Ascaris* shows that filament assembly and bundling move membranes. *Cell* 84:105-114.
- [4] Italiano J, Stewart M, Roberts T. 1999. Localized depolymerization of the major sperm protein cytoskeleton correlates with the forward movement of the cell body in the amoeboid movement of nematode sperm. *J. Cell Biol.* 146:1087-1095.
- [5] Italiano J, Stewart M, Roberts T. 2001. How the assembly dynamics of nematode major sperm protein generate amoeboid cell motility. *Intl. Rev. Cytol.* 202:1-34.
- [6] Lee J, Ishihara A, Theriot JA, Jacobson K. 1993. Principles of locomotion for simple-shaped cells. *Nature.* 362-11: 167-171.
- [7] LeClaire LL, Stewart M, Roberts T. 2003. A 48-kDa integral membrane phosphoprotein orchestrates the cytoskeletal dynamics that generate amoeboid cell motility in *Ascaris* sperm. *J. Cell Sc.* 116-13:2655-2663.
- [8] Miao L, Vanderlinde O, Stewart M, Roberts T. 2003. Retraction in amoeboid cell motility powered by cytoskeletal dynamics. *Science* 302-5649:1405-1407.
- [9] Mogilner A, and Oster G. 1996. Cell motility driven by actin polymerization. *Biophys. J.* 71:3030-3045.
- [10] Mogilner A, Verzi DW. 2003. A simple 1D physical model for the crawling nematode sperm cell. *J. Stat. Phys.* 110-316:1169-1189.
- [11] Mogilner A, Oster G. 2003. Shrinking gels pull cells. *Science* 302-5649:1340-1341.

- [12] Mogilner A. 2008. Mathematics of cell motility: Have we got its number? *J. Math. Bio.* (online first)
- [13] Roberts T, King KL. 1991. Centripetal flow and directed reassembly of the major sperm protein (MSP) cytoskeleton in the amoeboid sperm of the nematode, *Ascaris suum*. *Cell motility and the cytoskeleton.* 20-3:228-241.
- [14] Roberts T, Stewart M. 1995. Nematode sperm locomotion. *Cur. Op. in Cell Bio.* 7-1:13-17.
- [15] Roberts T, Stewart M. 2000. Acting like actin: The dynamics of the nematode major sperm protein (MSP) cytoskeleton indicate a push-pull mechanism for amoeboid cell motility. *J. Cell Biol.* 149-1:7-12.
- [16] Sepsenwol S, Taft SJ. 1990. In vitro induction of crawling in the amoeboid sperm of the nematode parasite, *Ascaris suum*. *Cell motility and the cytoskeleton.* 15-2:99-110.
- [17] Wolgemuth CW, Mogilner A, Oster G. 2004. The hydration dynamics of polyelectrolyte gels. *Eur. Biophys. J.* 33:146-158.
- [18] Wolgemuth CW, Miao L, Vanderlinde O, Roberts T, Oster G. 2005. MSP dynamics drives nematode sperm locomotion. *Biophys. J.* 88-4:2462-2471.
- [19] Yi K, BATTERY SM, Stewart M, Roberts TM. 2007. A Ser/Thr kinase required for membrane associated assembly of the major sperm protein motility apparatus in the amoeboid sperm of *Ascaris*. *Molecular Bio. of the Cell* 18-5:1816-1825.
- [20] Zajac M, Dacanay B, Mohler WA, Wolgemuth CW. 2008. Depolymerization-driven flow in nematode spermatozoa relates crawling speed to size and shape. *Biophys. J.* 94-10:3810-3823.

Fig. 1 Top and Side Views of Nematode Sperm Cell. (**Topview**) Schematic showing critical structures for spermatozoon of *A. suum*: (A) Points to leading edge of the lamellipod, (B) a membrane bound vesicle where the polymerization reactions take place, and (C) a cytoskeletal bundle which is assembled at the leading edge and disassembled closer to the cell body. (**Sideview**) Depicts spatial separation of protrusion/polymerization and contraction/depolymerization. The triangles along the bottom illustrate decreasing strength of adhesion from front to back. The nucleus and organelles are at the rear, with a relatively flat lamellipod at the front.

Fig. 2. Geometry of protrusion. Protrusion initiates at the set of points (x_{0_i}) , equally spaced along the leading edge of the cell body, using trigonometry to determine the slope of equiangular rays from the center of the cell. Protrusion of the cytoskeleton advances the gel forward as bundles advance rearward from intercollation of new dimers at the cell's edge. The direction for growth at point c is determined from graded protrusion along a vector normal to the secant line connecting points a and b . Over time, the tip of each bundle appears to glide rearward along the edge of the cell, so that the normal vector changes direction with curvature, and the bundles appear to bend. When the bundle at point b is absorbed near the cell body, the membrane protein at point d will initiate growth of a new cytoskeletal bundle, so that the total number of bundles is fixed over time.

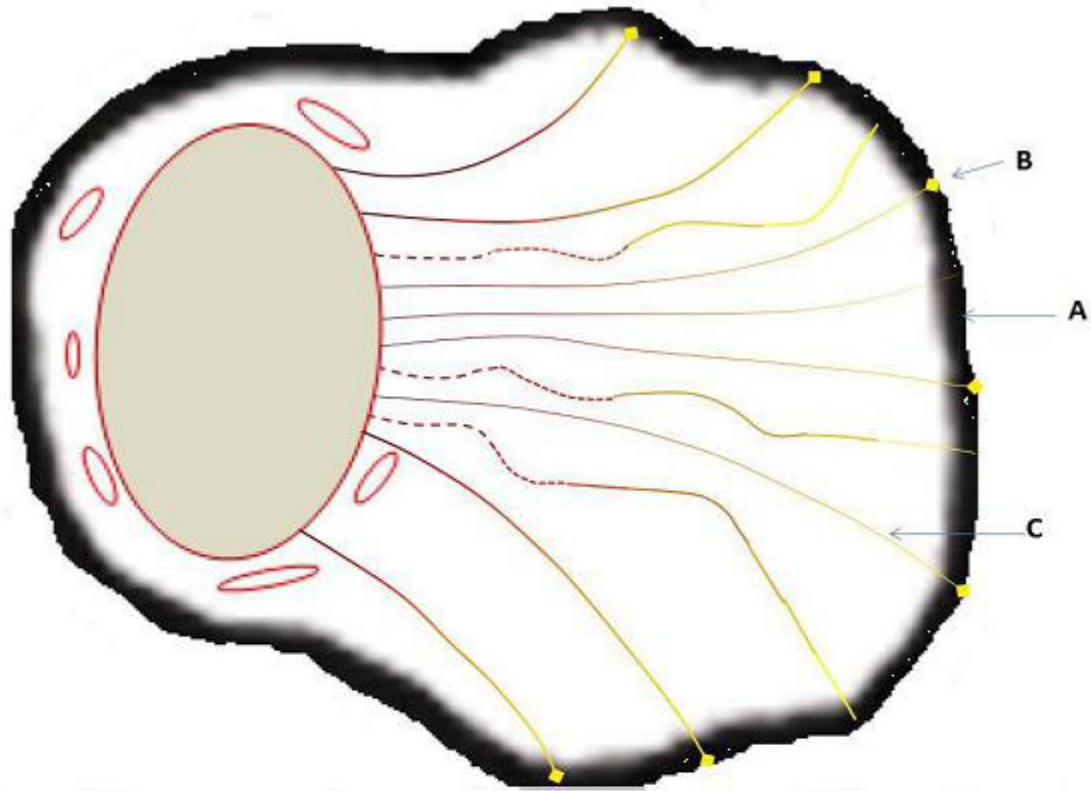
Fig. 3. Simulation for steady-state crawling. Graphs evolving contour of the lamellipod for a cell body with midrange curvature, $k = 0.5$ in Eq. (5). Simulation with nonlinear protrusion normal to the edge of the cell is graphed over four frozen moments in time. (**A**) At $t = 4$, the lamellipod extends but the cell body remains stationary. (**B**) After 14 units of time, the lamellipod is fully extended and the cell has moved one cell-length. (**C**) At $t = 24$, the lamellipod continues to crawl with a steady-state shape. (**D**) After 30 time units, the cell has migrated 2.5 cell lengths. While overall cell shape remains constant after extension, individual bundles recycle MSP dimers over space and time.

Fig. 4. Steady state shape. Results of three simulations for the crawling cell, varying initial shape, or curvature of the cell body from (k in Eq. (5)), and fixing 15 bundles per cell in each simulation. Slides on the left graph extension without cell body translocation after $t = 8$, while slides on the right show translocation and steady-state shape of the cell after $t = 30$. **(A)** A very flat cell body shape, ($k = 0.2$) tends to bunch MSP bundles in the direction of motion, resulting in translocation of 5 dimensionless units. **(B)** Midrange curvature ($k = 0.5$) results in more spatial separation between bundles in the direction of motion and a translocation of 5.25 dimensionless units. **(C)** A very curved cell body ($k = 0.8$) results in a relatively uniform distribution of bundles at steady-state, and a translocation of 4.25 spatial units. Maximum velocity over these simulations occurs for the cell with midrange curvature.

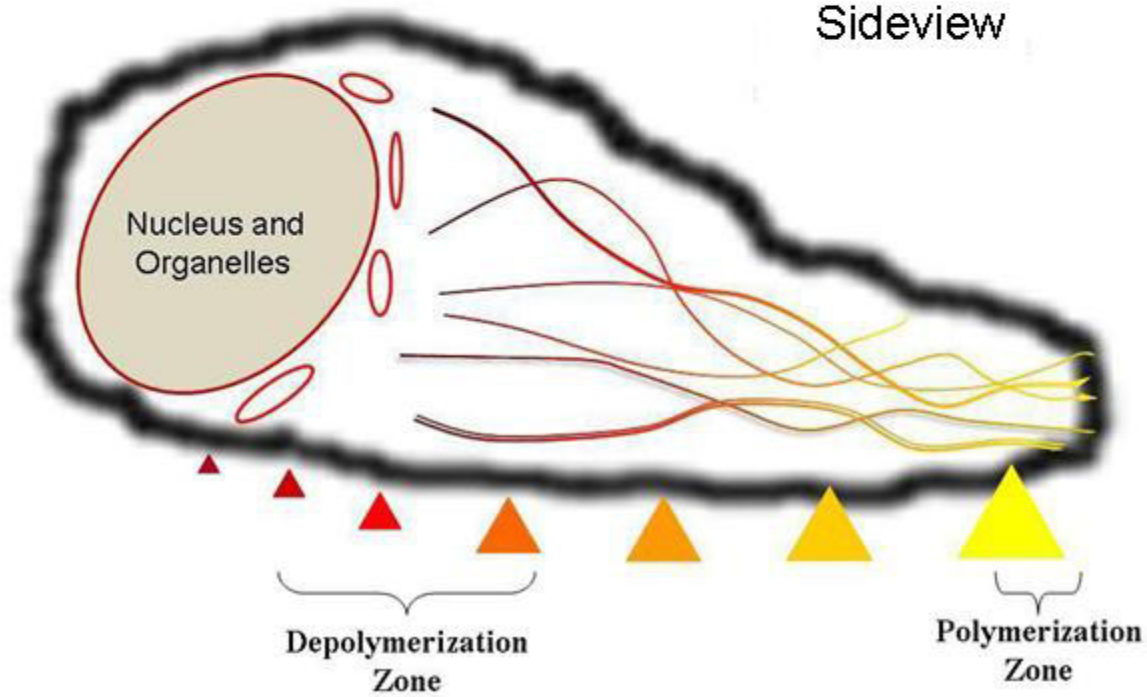
Fig. 5. Archival still shots of a turning sperm for *A. suum*. Reproduced, with permission, from video provided by T. M. Roberts, Florida State University. **(A)** The cell just before the turn: Note the small protrusion right and shadowed area of contraction left near the cell body. **(B)** The cytoskeleton has broken down in the lamellipod above the contraction area and the old leading edge appears to recede. **(C)** The cell body rotates to its new direction of motion. **(D)** Protrusion re-establishes the steady-state rectangular shape of the lamellipod, extending in the new direction of motion.

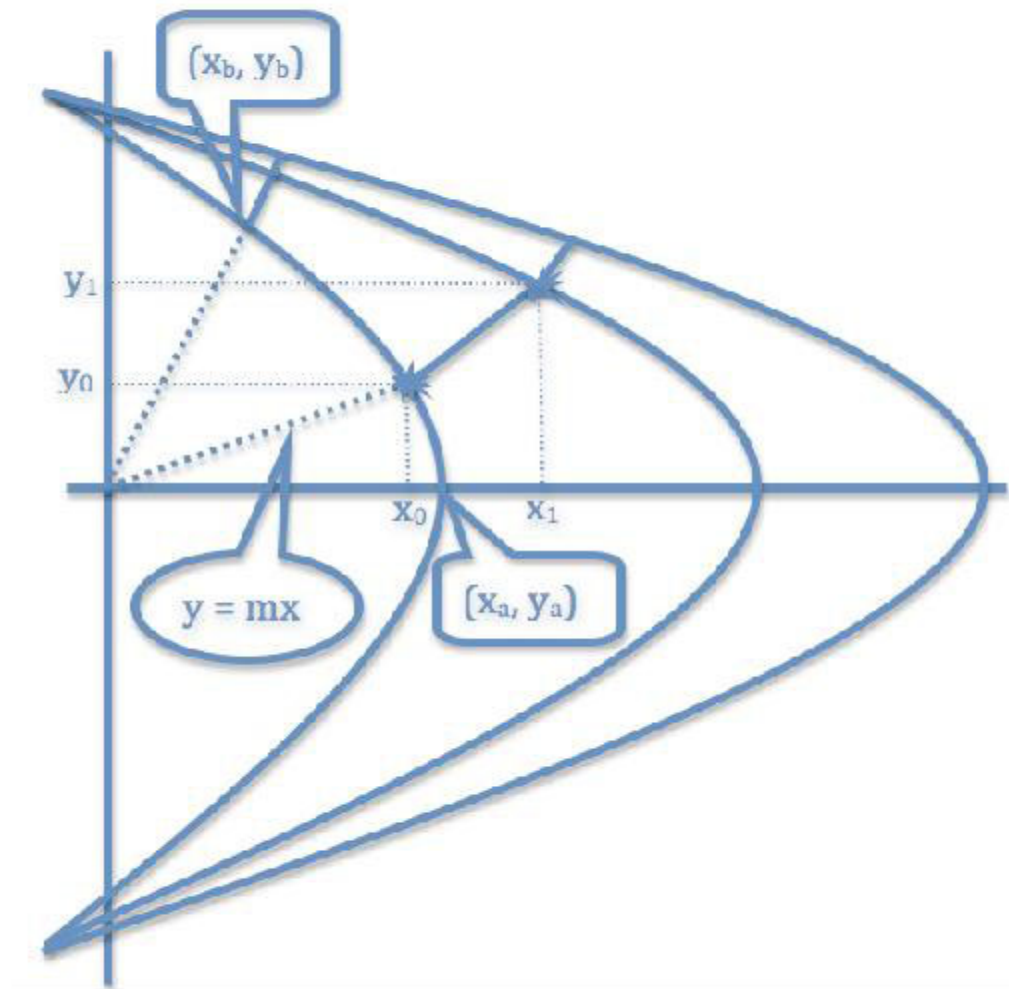
Fig. 6. Simulating the turning the cell. Images of the evolving contour, resulting from rotation of the cell body, and corresponding to rotation of the pH gradient, which, over time, affects the local rate of protrusion. **(A)** At $t = 4$, the lamellipod is protruding from a cell body with a high level of initial curvature. **(B)** After 11 time units, just prior to rotation, the cell body translocates behind the treadmilling lamellipod. **(C)** A slight rotation of the cell body occurs at $t = 12$, and we graph response at $t = 13$. Bundle symmetry has been broken so that bundles on the lateral left side are longer. **(D)** At $t = 16$, bundles on the left half of the cell have grown rapidly, and two new bundles have formed there, while bundles on the right side have stopped growing. The curvature of bundles on the lateral left side indicates a rapid change in the cell's contour, and a new leading edge for the lamellipod.

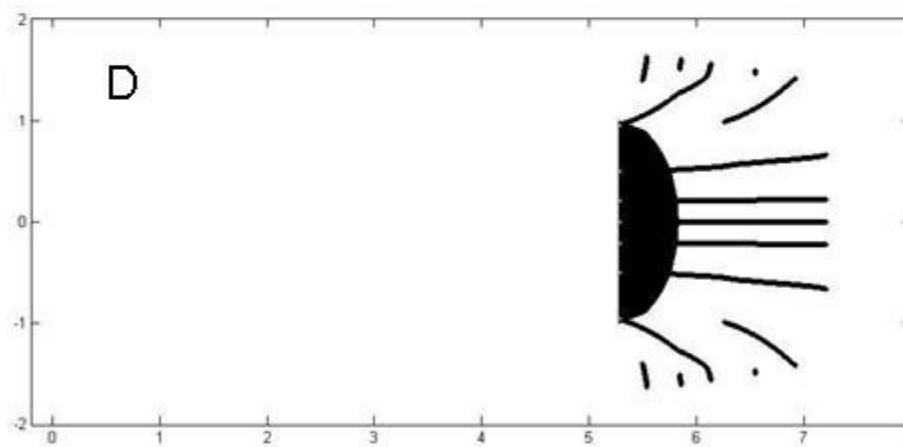
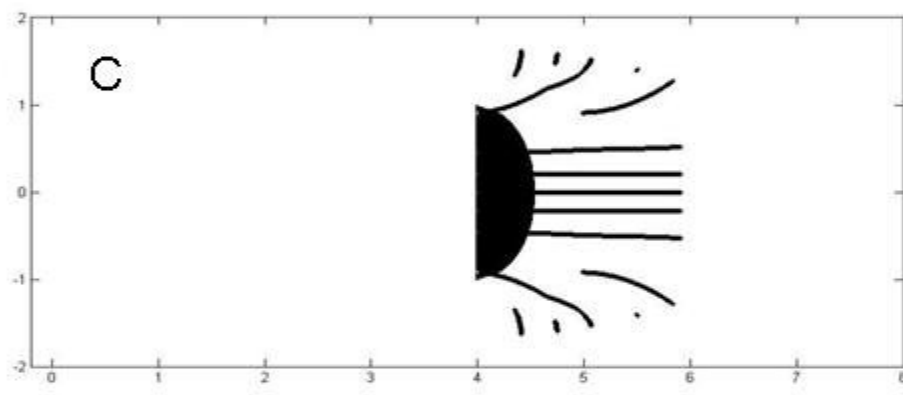
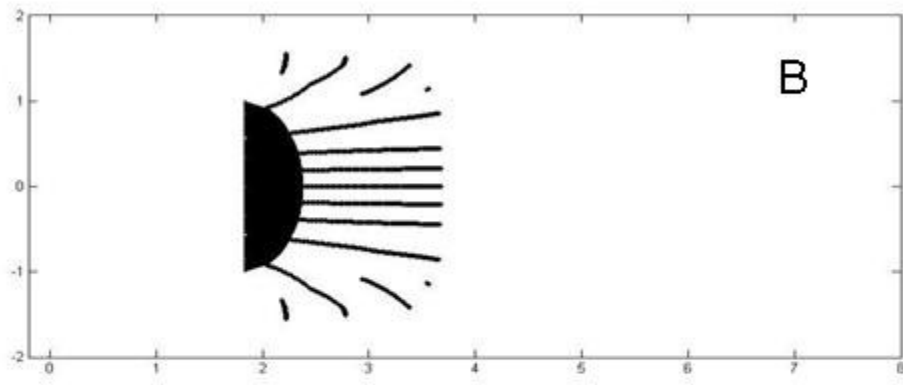
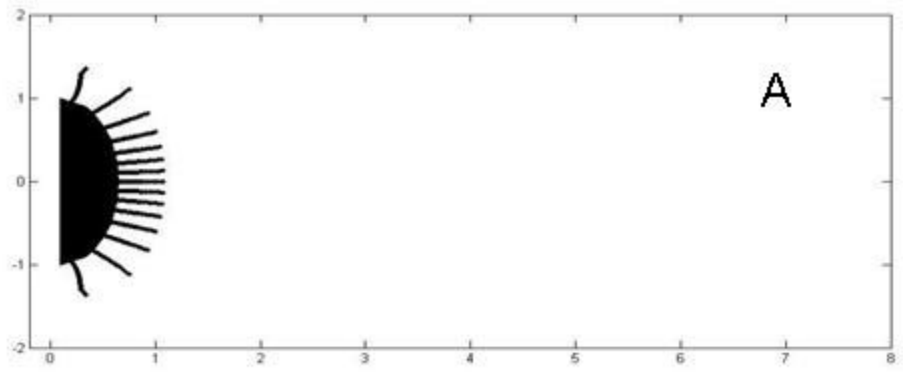
Topview



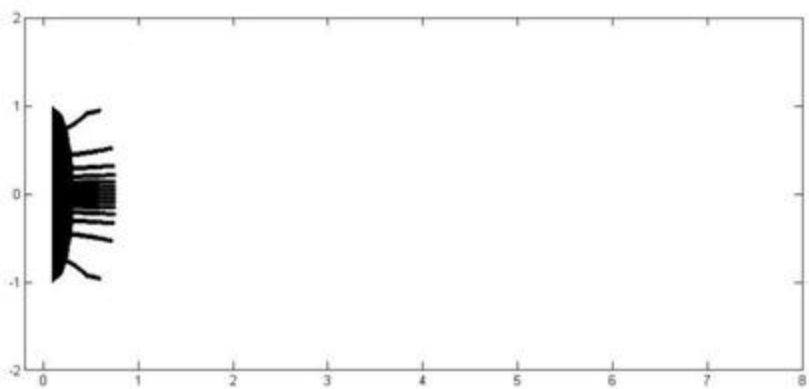
Sideview





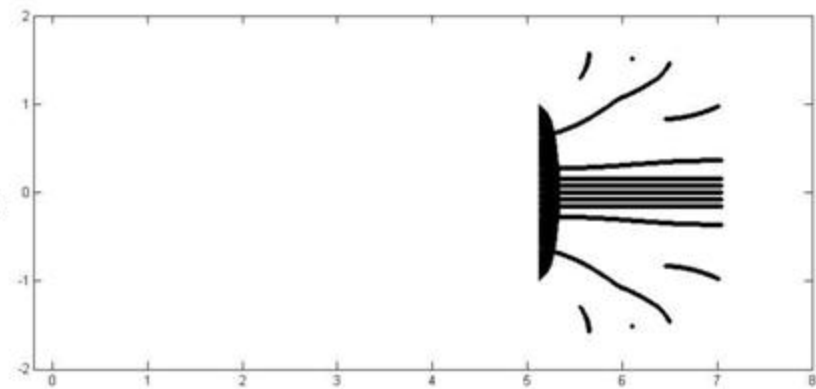


Starting Shape

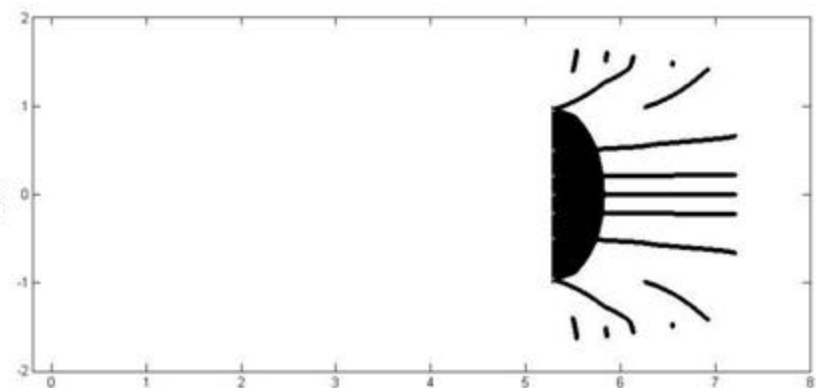
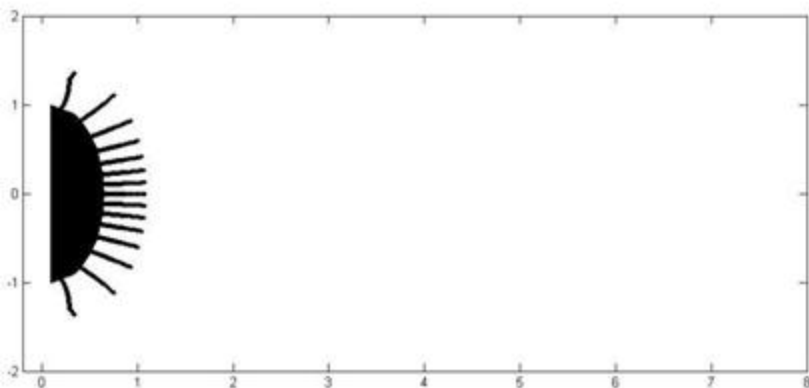


A

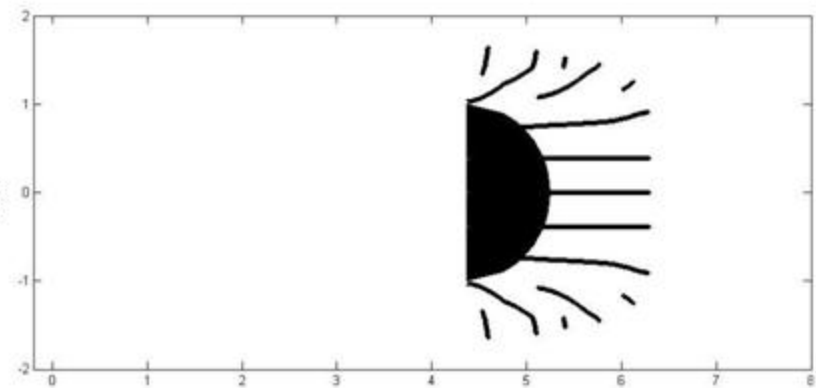
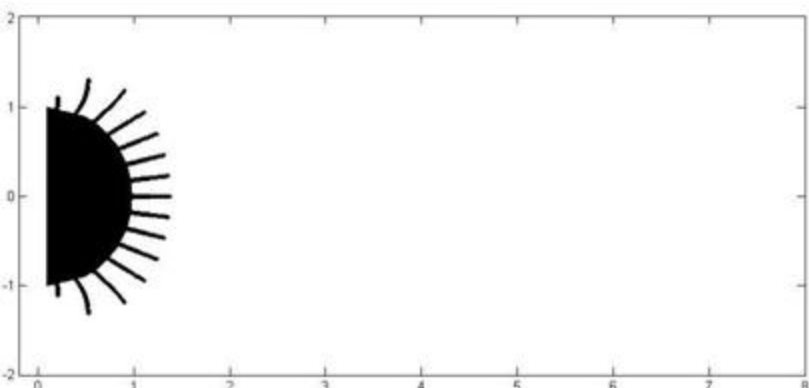
Steady State Shape



B



C



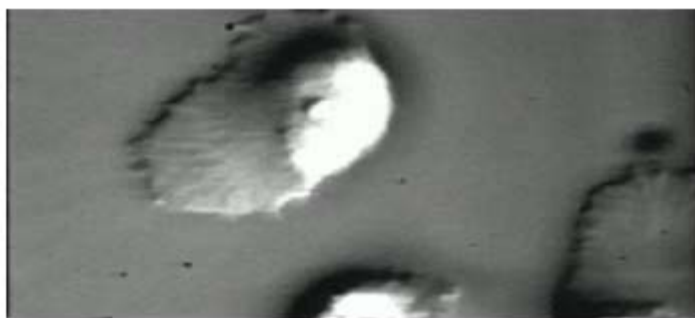
(A)



(B)



(C)



(D)



